

Evaluation of the linear mixing model in fluorescence spectroscopy

Peter Hoff¹ and Christopher Osburn²

¹Department of Statistical Science, Duke University

²Department of Marine, Earth, and Atmospheric Sciences, North
Carolina State University

December 20, 2024

Abstract

Analyses of spectral data often assume a *linear mixing hypothesis*, which states that the spectrum of a mixed substance is approximately the mixture of the individual spectra of its constituent parts. We evaluate this hypothesis in the context of dissolved organic matter (DOM) fluorescence spectroscopy for endmember abundance recovery from mixtures of three different DOM endmembers. We quantify two key sources of experimental variation, and statistically evaluate the linear mixing hypotheses in the context of this variation. We find that there is not strong statistical evidence against this hypothesis for high-fluorescence readings, and that true abundances of high-fluorescence endmembers are accurately recovered from the excitation-emission fluorescence spectra of mixed samples using linear methods. However, abundances of a low-fluorescence endmember are less well-estimated, in that the abundance coefficient estimates exhibit a high degree of variability across replicate experiments.

Summary: The impact of dissolved organic matter (DOM) on aquatic ecosystems is not always concentration-dependent: its sources matter. While the composition of DOM has been studied using sophisticated and cost-intensive chemical techniques, the light emitted by DOM, its fluorescence, is a rapid and cheap measurement technique that can fingerprint DOM’s sources in natural waters. However, fluorescence can only unravel a mixture of sources if the fluorescence of the mixture is approximately the same as a mixture of the source fluorescence. We evaluate this paradigm and confirm it holds for a range of DOM fluorescence profiles exhibited by most natural waters. However, we emphasize the need to make replicate measurements to confirm the reliability of the estimates made using linear unmixing methods.

1 Introduction

1.1 Scientific Background

Dissolved organic matter (DOM) in natural waters is a heterogeneous mixture of hundreds to thousands of individual compounds of varying molecular complexity and reactivity. DOM forms the basis of the microbial loop in natural waters and constitutes a major component of Earth’s carbon cycle, while also influencing water quality in lakes, streams, groundwater, rivers, and estuaries and coastal waters. Along the hydrologic networks of the Earth’s surface connecting land to ocean, DOM originates from a variety of sources such as natural organic matter stored in surface plant litter and soils, produced within natural waters via primary and secondary production, and exchanged between adjacent ecosystems. Further, DOM is generated in the built environment and can be discharged into natural waters as domestic and industrial sewage as well as runoff from human modifications to the landscape from urbanization and agriculture (e.g., Wilson and Xenopoulos [2009], Bhattacharya and Osburn [2020]).

Unraveling the mixture of DOM sources is important because DOM’s biogeochemical reactivity reflects its composition (i.e., quality) as much as its concentration (quantity). DOM’s reactivity in natural waters is important because the degree to

which it can be utilized by microorganisms can influence water quality – potentially contributing to eutrophication, hypoxia, and acidification. For researchers and practitioners alike, understanding the reactivity of DOM by characterizing its quality and then apportioning its sources in a mixture is important.

Several approaches have been utilized to characterize DOM’s quality, and chief among them is its light absorbing and fluorescing properties, collectively termed the chromophoric portion of DOM – CDOM. These spectral properties of DOM can be measured rapidly (within a few hours of collection) on cost-effective instruments. While they do not elucidate the molecular composition specifically, CDOM absorbance and fluorescence do provide a great deal of information about its sources [Fellman et al., 2010, Stedmon and Nelson, 2015].

Across the land to ocean aquatic continuum (LOAC), DOM can be thought of as a mixture of several sources. Thus, with prior knowledge of the possible sources to a particular downstream location in a river or to receiving waters such as lakes and estuaries, it should be possible to unravel the components of the mixture. For example, endmember mixing models assume that runoff in a catchment is a mixture of unique sources whose contributions can be determined using tracers that exhibit conservative behavior, even if they integrate processes occurring in a watershed [Inamdar, 2011, Larsen et al., 2015]. Prior work with CDOM fluorescence as a conservative tracer of DOM sources has utilized parallel factor analysis (PARAFAC) decomposition [Bro, 1997, Osburn et al., 2016] and least squares regression [Goldman et al., 2012], and endmember mixing analysis (EMMA) based on mass balance [Derrien et al., 2018, Lee et al., 2020]. Recent work by Bryan et al. [2023, 2024] provides a simple least squares regression approach (“Regress-Then-Sum”, RTS) that add to the methodology available for DOM source unmixing. Uncertainty in the measurement of CDOM fluorescence has been addressed [Murphy et al., 2010, Korak et al., 2014]. Implicit in these unmixing methods is the linear mixing hypothesis, which assumes that the fluorescence profile of a mixed sample resembles the mixed profile of its source components. This concept constitutes the rationale of the mass balance approach. In theory, a DOM sample taken along the LOAC is a mixture of the sources upstream to it. The mass balance approach requires, for example, that in

a river network the fractions of the upstream endmembers in a downstream sample must sum to 1. However, each source and the resulting mixture carry some environmental history including microbial or photodegradation, adsorption or desorption onto or from particles, binding to metals, among others [Lee et al., 2018]. Thus a mixed water sample will be a mixture of these upstream sources and the processing these upstream sources experience prior to sample collection. (In tidal systems, we may also consider ocean sources.) We may also represent source categories by measuring fluorescence on representative samples collected from a particular source and incorporating its environmental history. In principle, this means we can define a collection of fluorescence observations measured within source categories (i.e., a dictionary). With this framework in mind, we can now formalize the source mixing problem based on fluorescence. It can be expected that DOM samples with substantial measurable signal will follow this assumption because the magnitude of experimental variation will be much lower than the signal itself. However, a key question to answer is if the experimental variation for samples with fluorescence signals near the limit of detection is small enough make the linear mixing hypothesis useful in practice. This is important to establish, in particular when mixing problems must resolve very small individual contributions of sources (e.g., a few percent). Thus, to evaluate the utility of the linear mixing hypothesis as applied to CDOM fluorescence there is a need to identify the range of fluorescence signals for which the hypothesis is likely to hold and be practically useful for reliable estimation of mixing proportions.

1.2 Statistical Background

As described below in Section 2, CDOM profiles of water samples are obtained by measuring fluorescence at combinations of multiple excitation and emission frequencies. These fluorescence measurements are generally arranged to form an excitation-emission matrix, or EEM. Each excitation/emission pair in the EEM is referred to as a *pixel*. For mathematical and statistical calculations, it is often useful to rearrange the entries of an EEM as a vector, which we refer to as the *vectorization* of the EEM.

Let μ be a vectorization of a hypothetical EEM from a mixed water sample

that is measured with no replication or measurement error, and similarly define $\theta^k, k = 1, \dots, s$ as noiseless vectorized EEMs of potential endmembers of the sample. If the abundances of the endmembers in the mixed sample are given by b_1, \dots, b_s , then the linear mixing hypothesis states that

$$\mu \approx \Theta b = \theta^1 b_1 + \dots + \theta^s b_s,$$

where Θ is a matrix with columns $\theta_k, k = 1, \dots, s$, b is a vector with elements b_1, \dots, b_s , and Θb is the matrix-vector product of Θ and b . Deviations from the linear mixing hypothesis could be evaluated, pixel by pixel, by examining the elements of the vector $\mu - \Theta b$.

Due to variation in experimental procedures and noise from measurement devices, the exact values of μ and $\theta^1, \dots, \theta^s$ are unavailable. Instead, we have noisy measurements of these vectors, from which we obtain estimates $\hat{\mu}$ and $\hat{\theta}^1, \dots, \hat{\theta}^s$. The linear mixing hypothesis can be evaluated by comparing $\hat{\mu}$ to $\hat{\Theta} b$, but even if the hypothesis is true we do not expect these quantities to be exactly equal, because $\hat{\mu}$ and $\hat{\Theta}$ are not exactly equal to μ and Θ due to experimental noise and variation. To evaluate the linear mixing hypothesis using $\hat{\mu}$ and $\hat{\Theta} b$, we need to compare the values of their difference to the range of plausible values, accounting for experimental variation.

1.3 Outline of This Study

In Section 2 we describe an experiment conducted to quantify the sources of experimental variation in fluorescence measurements of several mixed water samples obtained from three known sources of DOM in the Neuse River basin, eastern North Carolina: groundwater, streamwater, and wastewater. These sources represent a gradient of CDOM concentrations common in natural waters of the LOAC [Mascotte et al., 2017]. From our experimental results, in Section 3 we identify and quantify two primary sources of experimental variation, which we refer to as procedural variation and measurement variation. The degree of procedural variation among the water samples is fairly consistent, but the degree of measurement variation appears to be signal-dependent. Specifically, our groundwater samples with

very low amounts of fluorescence near the limit of detection exhibit a much lower signal-to-noise ratio than the other samples. Using estimates of these sources of variation, we statistically evaluate the linear mixing hypothesis in Section 4, and find little evidence of violations of the hypothesis for most combinations of excitation and emission wavelengths, especially for pixels with strong emission signals. We also evaluate the precision of the linear mixing model for endmember abundance estimation, by comparing the true endmember abundances in a mixed water sample to estimated abundance coefficients. For the water samples analyzed in this study, the abundances of high-fluorescence endmembers are precisely estimated, whereas abundance estimates for the low-fluorescence groundwater endmember are less precise. A discussion of results and recommendations follow in Sections 5 and 6.

2 Materials and Procedures

We evaluated the linear mixing hypothesis using mixtures of three endmember water samples, including a groundwater sample, a streamwater sample and a wastewater sample. These samples were collected in late April and early May of 2024. The groundwater sample was collected from a residential well in Wake County, NC. The streamwater sample was collected from a walking bridge over Rocky Branch, a stream located on NC State’s campus. The wastewater sample was collected as a 24-hour composite sample of domestic and industrial sewage in the influent entering the Corpening Creek Wastewater Treatment Plant in Marion, NC. All three samples were collected in detergent-cleaned brown HDPE bottles and stored at 4 °C in the dark until transported to the laboratory. Samples were then filtered through pre-combusted (450 °C for six hours) Cytiva Whatman glass fiber filters (GFF; 0.7 μm mesh size) into detergent-cleaned polycarbonate bottles and stored in a refrigerator until measurement. The wastewater was diluted (1:2 vol/vol) with ultrapure water (MilliQ, 18.2 M Ω resistivity) prior to filtration. Dilution was accounted for when fluorescence was corrected as described below.

The three different source water samples, or endmembers, were mixed in various

Sample	% Groundwater	% Streamwater	% Wastewater
s_1	1.00	0.00	0.00
s_2	0.00	1.00	0.00
s_3	0.00	0.00	1.00
m_1	0.00	0.50	0.50
m_2	0.50	0.50	0.00
m_3	0.50	0.00	0.50
m_4	0.25	0.25	0.50
m_5	0.25	0.50	0.25
m_6	0.50	0.25	0.25
m_7	0.33	0.33	0.33

Table 1: Mixture weights (abundances) of endmembers of the ten water samples.

proportions to obtain seven different mixed water samples (Table 1). These mixtures represent examples of problems where we wish to determine the relative proportions of a mixture. For example, contamination of wastewater in streamwater or the relative exchange between groundwater seepage discharging into a stream. For each of the $s = 3$ source samples and $m = 7$ mixed samples, $n = 3$ replicate aliquots (subsamples) were obtained and scanned. For all dilutions and sample transfers, a laboratory pipette (Gilson Pipettman) with polypropylene tips were used. The pipette tips were rinsed with Milli-Q water prior to use. Measurement of Milli-Q water transferred with the pipette revealed no contamination of absorbance or fluorescence by the tips.

Absorbance of each aliquot was scanned first from 200 to 800 nm in a 1 cm quartz cell (Starna) using a Varian Cary 300UV spectrophotometer. Milli-Q water was scanned separately and used as a blank. CDOM absorption values were computed as $a_\lambda = (A_{\lambda,\text{sample}} - A_{\lambda,\text{blank}})/L$, where a is the Napierian absorption coefficient, A is the unitless absorbance measured on the spectrophotometer, λ is the wavelength in nm, and L is the pathlength of the quartz cell, in meters. The mean and standard deviation of the CDOM absorption at 350 nm, a common expression of CDOM

Sample	Mean	Standard deviation
Groundwater	0.73	0.44
Streamwater	7.92	0.41
Wastewater	16.20	0.12

Table 2: Mean and standard deviation of CDOM absorption values at 350 nm (units of inverse meters, m^{-1}) for the three samples used in this study.

concentration in natural waters is given in Table 2. These values fall within the large range of CDOM values for natural waters across the LOAC [Massicotte et al., 2017]. CDOM fluorescence is measured as emission (Em) intensity over a wavelength range of constant interval at a fixed excitation (Ex) wavelength, creating multiple emission spectra, which get arranged to form an excitation-emission matrix (EEM) as described in Section 1.2. EEMs are most commonly viewed as contour plots or “landscapes” that visualize the strength of emission intensity in different regions of EEM-space. Fluorescence emission from 300 to 600 nm at 2 nm increments was then measured at excitation wavelengths from 240 to 450 nm at 5 nm increments using a Varian Eclipse spectrophotometer. This procedure resulted in a 151×43 -dimensional EEM for each of the $30 = n \times (s+m)$ subsamples, representing fluorescence intensities at 151 emission wavelengths and 43 excitation wavelengths. For each EEM, the Milli-Q blank was subtracted, and then corrections applied for variability in excitation lamp spectra and detector response and inner filter effects [Kothawala et al., 2013]. Emission was normalized to the instrument’s water Raman signal and then calibrated to quinine sulfate units where $1 \text{ QSU} = 1 \mu\text{g/L}$ quinine sulfate dissolved in 0.1 M sulfuric acid [Gilchrist and Reynolds, 2014]. Common absorbance and fluorescence properties of each source and mixture, including all replicates, are presented in the Supporting Information in Table S1. Representative contour plots of the source and mixture EEMs are also provided in the Supporting Information.

The physically meaningful entries of an EEM correspond to the $p = 5065$ excitation/emission pairs, or pixels, for which the emission wavelength is longer than the excitation wavelength. The p -dimensional vector of fluorescence intensities of an

EEM at these pixels is the vectorization of the EEM. The statistical analyses that follow are based on the vectorizations of these 30 EEMs, and so the dataset consists of 30 p -dimensional vectorized EEMs, three for each of the ten water samples listed in Table 1. All analyses were performed using R Statistical Software [R Core Team, 2024, v4.4.1]. Data and replication code for the numerical results in this article are available at http://www.stat.duke.edu/~pdh10/Code/hoff_osburn_2024

3 Assessment of Experimental Variation

3.1 Procedural Variation

First we investigate the variation across the $n = 3$ replicate EEMs for each of the 10 water samples. Let y_i be the p -dimensional vectorized EEM of the i th replicate from one of the mixed water samples, and let x_i be the vectorized EEM of the i th replicate from one of the endmember water samples. We expect replicate EEMs from a common water sample to resemble each other, and thus to also resemble their within-sample average. Notationally, this means we expect that $y_i \approx \bar{y}$ and $x_i \approx \bar{x}$ for $i = 1, \dots, n$, where for example $\bar{x} = \sum_i x_i/n$ is the p -dimensional vector obtained by averaging the replicate values at each pixel (i.e., \bar{x} is the “average EEM” of an endmember).

This approximation is examined empirically for two of the mixture samples (m_1 and m_2) in Figure 1. Mixture m_1 was 50:50 (vol/vol) of the streamwater and the wastewater, respectively. Mixture m_2 was 50:50 (vol/vol) of the streamwater and the groundwater. The figure shows a strong linear correlation between each replicate EEM and the average EEM for its water sample. However, notice that the fluorescence values in several of the scatterplots are slightly but consistently above or below the green 45 degree line, indicating that the pixels of one replicate can have values systematically higher or systematically lower than those of another from the same water sample.

A more comprehensive evaluation of this phenomenon is given in Table 3. The first three columns are the linear correlations between each average EEM and the

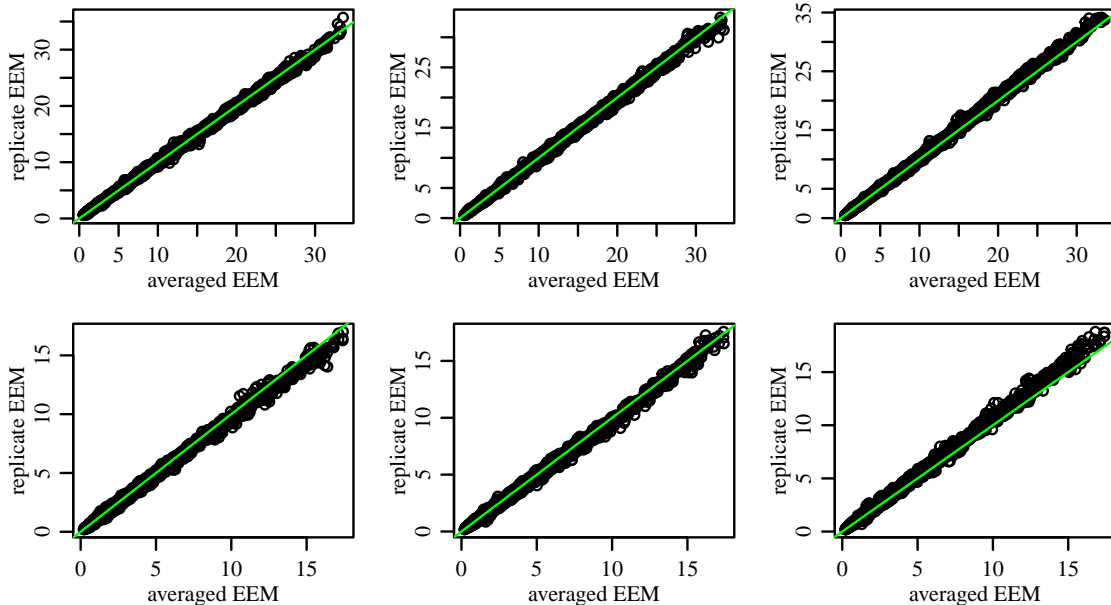


Figure 1: Replicate versus average EEMs for two mixed water samples. The top row is mixture m_1 (streamwater and wastewater), the bottom row is mixture m_2 (streamwater and groundwater).

replicate EEMs that make up the average. For example, the first three columns give for each row the across-pixel sample correlations $\hat{\rho}_1, \hat{\rho}_2, \hat{\rho}_3$ between \bar{y} and y_1, y_2, y_3 respectively (or between \bar{x} and x_1, x_2, x_3 for an endmember water sample). The correlation coefficients are all nearly 1, except for the replicates from the groundwater sample s_1 .

The second three columns of the table give the across-pixel average ratio of a replicate EEM to its corresponding average. For example, in each row the coefficient \hat{a}_i is given by $\hat{a}_i = \sum_j (y_{i,j} / \bar{y}_j) / p$, where i indexes replicates and j indexes pixels. Across the table, the a -values range from 0.941 to 1.064, and thus vary by as much as 6% from 1. The final column of Table 3 gives $\hat{\sigma}_a$, the sample standard deviation of these average ratios, that is, the sample standard deviation of the preceding three columns of the table. This number quantifies how much the pixel values in a replicate EEM may be systematically larger or smaller than those of the sample average EEM.

	$\hat{\rho}_1$	$\hat{\rho}_2$	$\hat{\rho}_3$	\hat{a}_1	\hat{a}_2	\hat{a}_3	$\hat{\sigma}_a$
s_1	0.903	0.908	0.882	1.015	0.955	1.026	0.038
s_2	0.999	0.999	0.999	0.991	0.989	1.020	0.017
s_3	1.000	1.000	1.000	1.034	0.973	0.992	0.031
m_1	0.999	0.999	0.999	1.016	0.983	1.001	0.016
m_2	0.998	0.998	0.999	0.966	0.970	1.064	0.056
m_3	0.999	0.999	0.999	0.966	1.042	0.992	0.039
m_4	0.999	0.999	0.999	0.990	1.026	0.984	0.023
m_5	0.999	0.999	0.999	0.941	1.039	1.020	0.052
m_6	0.999	0.999	0.999	0.942	1.049	1.010	0.054
m_7	0.999	0.999	0.999	0.942	1.029	1.029	0.050

Table 3: EEM-level multiplicative variation among water samples. Rho ($\hat{\rho}$) is the Pearson’s correlation coefficient, \hat{a} is the across-pixel average ratio of a replicate to its mixture’s average, and $\hat{\sigma}_a$ is the standard deviation of the average ratios.

A replicate EEM with a high \hat{a} -value indicates that, on average across pixels, its fluorescence values are higher than those of the other replicates from the same water sample. Possible explanations of this phenomenon include variation in the amount of Milli-Q water added for dilution, variation in residual water in a sample container, and possibly other slight variations in experimental procedures that involve use of the Gilson Pipetteman pipette. We refer to this variation as *procedural variation*, and model this variation mathematically with the multiplicative approximation given by

$$y_i \approx a_i \times \mu,$$

where μ is a p -dimensional perfectly-measured “true” EEM, and a_i is a scalar representing how much the overall fluorescence of an observed EEM y_i varies as a fraction of that of μ . The values a_1, \dots, a_n can be viewed as multiplicative error terms that vary around the value of 1. An estimate of μ is given by $\hat{\mu} = \bar{y}$, and as described above, we estimate each a_i as $\hat{a}_i = \sum_j (y_{i,j} / \hat{\mu}_j) / p$. Because the values of $\hat{\sigma}_a$ do not vary considerably across the samples, in the analyses that follow we use a single pooled estimate of $\hat{\sigma}_a \approx 0.04$, or equivalently, $\hat{\sigma}_a^2 \approx 0.0016$.

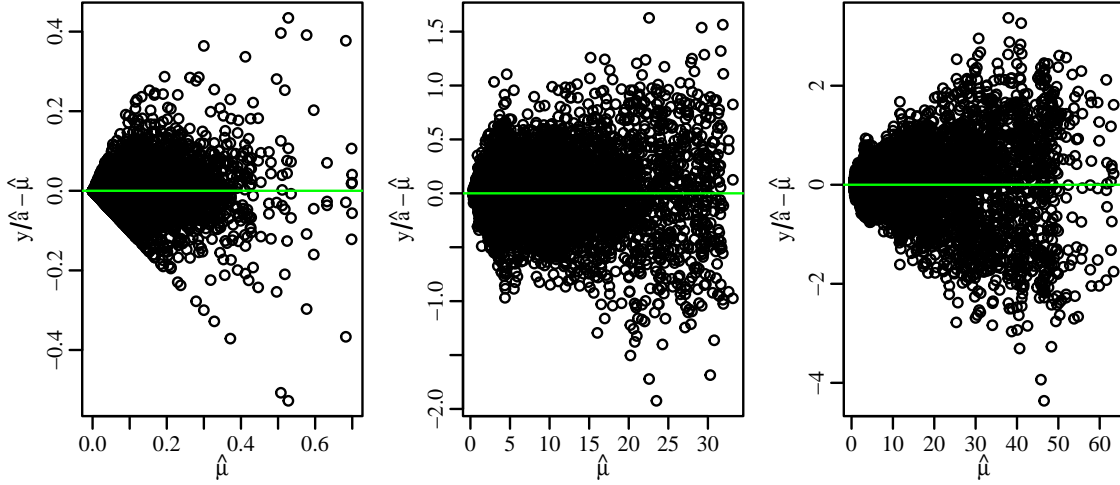


Figure 2: Fitted versus residual plots for s_1 , s_2 and s_3 .

3.2 Measurement Variation

In the previous subsection we examined the approximation $y_i \approx a_i \mu$ where μ is an unknown perfectly-measured EEM vector for a given water sample, and a_i is single number that scales the entire μ -vector up or down. We estimated each a_i by first estimating μ with the sample average vector $\hat{\mu} = \sum_i y_i/n$, and then letting $\hat{a}_i = \sum_j (y_{i,j}/\hat{\mu}_j)/p$. Based on the above approximation we have $y_i/a_i \approx \mu$ and so we expect that $y_i/\hat{a}_i \approx \hat{\mu}$. However, even after accounting for the across-replicate multiplicative variation represented by variation in a_1, \dots, a_n , there is still pixel-to-pixel variation. Some of this variation is displayed graphically in Figure 2, which for the three endmember water samples (s_1 , s_2 and s_3), plots the difference between each scale-adjusted EEM y_i/\hat{a}_i and the sample average $\hat{\mu}$, as a function of $\hat{\mu}$. These “residuals” of the scaled replicate EEMs vary around zero by an amount that increases with the magnitude of the average signal. In other words, the residual variance for high-fluorescence pixels is higher than that of low-fluorescence pixels. This kind of mean-variance relationship is common for non-negative data types such as fluorescence data.

This mean-variance relationship can be quantified numerically by comparing the

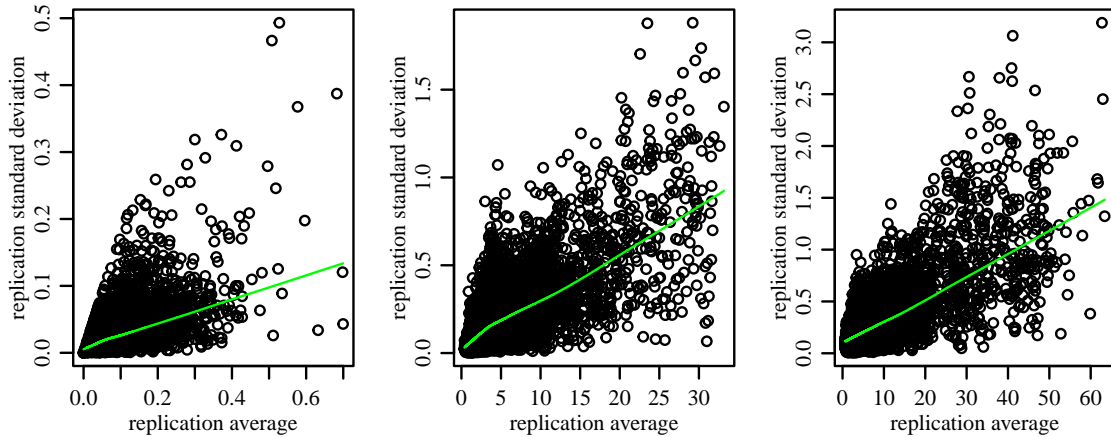


Figure 3: Sample replication standard deviation versus sample replication average across pixels for water samples s_1 , s_2 and s_3 .

sample mean and sample standard deviation of the three replicate values at each pixel and for each endmember water sample. This relationship is shown graphically in Figure 3. Each point in each of the three plots gives the sample mean and sample standard deviation of one of the p pixels. The green curve in each figure is a smooth approximation of the functional relationship between the mean and the standard deviation. While noisy due to the small sample size ($n = 3$ at each pixel), there is a clear positive mean-variance relationship that looks approximately linear, on average across pixels. The pattern looks similar for the seven other water samples that were mixtures of the three endmembers.

A linear relationship between the mean of a random variable and its standard deviation can be modeled with multiplicative error, rather than the usual additive error assumed in most statistical models. Specifically, if we use the model

$$y_{i,j} = a_i \mu_j e_{i,j} \quad (1)$$

where $e_{i,j}$ has a mean of one and a standard deviation σ_e , then the standard deviation

	$\hat{\sigma}_e$	$\hat{\text{SNR}}$
s_1	0.155	6.358
s_2	0.002	279.789
s_3	0.003	230.323
m_1	0.002	264.960
m_2	0.004	188.193
m_3	0.005	154.957
m_4	0.003	234.333
m_5	0.002	251.058
m_6	0.004	194.279
m_7	0.003	229.615

Table 4: Sample-specific estimates of σ_e (first column) and SNR (second column).

of a scaled EEM measurement $y_{i,j}/a_i$ is

$$\begin{aligned} \text{SD}[y_{i,j}/a_i] &= \text{SD}[\mu_j e_{i,j}] \\ &= \mu_j \text{SD}[e_{i,j}] = \mu_j \sigma_e, \end{aligned}$$

and so the standard deviations across pixels $j = 1, \dots, p$ will be linearly related to the means, with slope given by σ_e .

Estimates of σ_e can be obtained by computing the standard deviation of the multiplicative residuals $\hat{e}_{i,j}$, given by

$$\hat{e}_{i,j} = y_{i,j}/(\hat{a}_i \hat{\mu}_j).$$

Separate estimates of σ_e for each water sample are given in Table 4. The values are similar across all water samples except for s_1 , the groundwater endmember sample, having a standard deviation nearly an order of magnitude larger than the others.

The estimates of σ_e can be combined with the estimate of σ_a to obtain signal to noise ratios for each of samples. Based on the multiplicative model (1), the variance of $y_{i,j}$ is given by

$$\text{Var}[y_{i,j}] = \mu_j^2 \times ((\sigma_a^2 + 1) \times (\sigma_e^2 + 1) - 1), \quad (2)$$

and so the signal-to-noise ratio (SNR) for a given water sample is

$$\text{SNR} = \mu_j^2 / \text{Var}[y_{i,j}] = \frac{1}{(\sigma_a^2 + 1) \times (\sigma_e^2 + 1) - 1}$$

Estimates of the SNR for each water sample are given in the second column of Table 4, using the common estimate of $\hat{\sigma}_a^2$ described in the previous subsection and the sample-specific estimates of σ_e^2 from the first column of the table. Note the extremely low SNR of the groundwater sample, relative to those of the other two.

4 Evaluating the Linear Mixing Model

4.1 Testing the Linear Mixing Hypothesis

Recall from the Introduction that the linear mixing hypothesis states that for each pixel j ,

$$\mu_j \approx \theta_j \cdot b = \theta_j^1 b_1 + \dots + \theta_j^s b_s$$

where $\theta_j = (\theta_j^1, \dots, \theta_j^s)$ is the vector of fluorescence values at pixel j of the s endmember EEMs. In this subsection, we statistically test the hypotheses $H_j : \mu_j = \theta_j \cdot b$, separately for each $j = 1, \dots, p$ and each of the seven mixed water samples, using the following multiplicative model developed in the previous section:

- $y_{i,j} = a_i \mu_j e_{i,j}$ for $i = 1, \dots, n$;
- a_1, \dots, a_n are independent and identically distributed (i.i.d.) random variables with mean 1 and variance σ_a^2 ;
- $e_{1,j}, \dots, e_{n,j}$ are i.i.d. random variables with mean 1 and variance σ_e^2 ;
- the a_i 's and $e_{i,j}$'s are independent.

We also assume the same model holds for the replicates $x_{1,j}^k, \dots, x_{n,j}^k$ for each endmember $k = 1, \dots, s$.

Let $\hat{\theta}_j = \bar{x}_j = (\bar{x}_j^1, \dots, \bar{x}_j^s)$ be the vector of average fluorescence values for each of the s endmembers at pixel j , and similarly let $\hat{\mu}_j = \bar{y}_j = \sum_i y_{i,j} / n$ be the sample

average for a mixed water sample at pixel j . Under the model described above, $\hat{\theta}_j$ is an unbiased estimate of θ_j , and $\hat{\mu}_j$ is an unbiased estimate of μ_j . Evidence against the hypothesis $\mu_j = \theta_j \cdot b$, or equivalently $\mu_j - \theta_j \cdot b = 0$, may be quantified by how far the estimate $\hat{\mu}_j - \hat{\theta}_j \cdot b$ is from zero, relative to its standard deviation. Specifically, we evaluate H_j with the z -statistic

$$z_j = \frac{\hat{\mu}_j - \hat{\theta}_j \cdot b}{\hat{\sigma}_j}$$

where $\hat{\sigma}_j$ is an estimate of the standard deviation of the numerator in the above expression, and is derived in the Supporting Information. Under the model assumptions, if the linear mixing hypothesis is correct then the numerator of z_j should have a mean of zero and be approximately normally distributed by the central limit theorem. Dividing by an estimate of the standard deviation provides us with a test statistic z_j that should be approximately normally distributed under the linear mixing hypothesis. Thus a statistical test of $H_j : \mu_j = \theta_j \cdot b$ may be performed by comparing z_j to a standard normal distribution.

For each of the m mixed samples we computed a z -score z_j and the associated p -value p_j for each pixel $j = 1, \dots, p$. Significant deviations from the linear mixing hypothesis were evaluated using the Benjamini-Hochberg (BH) algorithm [Benjamini and Hochberg, 1995] with a false discovery rate (FDR) of $\alpha = .05$ to account for the fact that we are evaluating $p = 5065$ hypotheses for each mixed sample. Pixels having p -values below the BH threshold are indicated in Figure 4, with blue and yellow indicating pixels with lower and higher than expected fluorescence, respectively. Across samples, the number of such pixels was roughly 2% or less of the total number of pixels. Most of the the pixels that indicated some violation of the hypothesis had low-fluorescence measurements, although for most low-fluorescence pixels there is no strong evidence of the hypothesis being violated. Moreover, the region of fluorescence where some violation of the hypothesis was indicated (emission wavelengths ≥ 500 nm) typically lacks DOM source information.

The relationship between fluorescence and evidence against the linear mixing hypothesis is shown in the bottom-right panel of Figure 4, which plots the p -value for

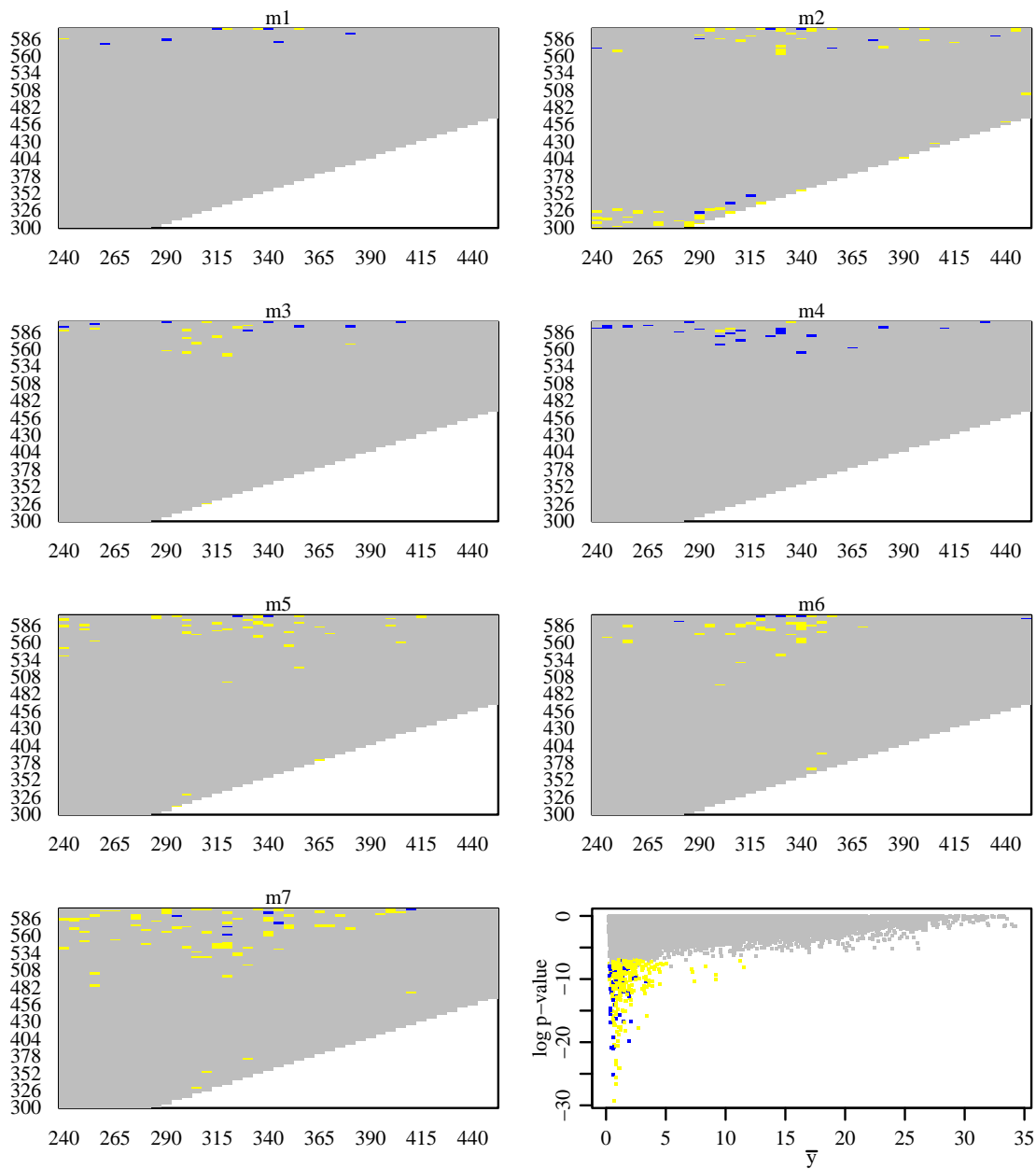


Figure 4: Pixel-specific tests of the linear mixing hypothesis using the BH threshold with FDR = 0.05. Blue and yellow pixels indicate fluorescence of a mixed pixel as significantly lower and higher than expected under linear mixing, respectively. The bottom-right panel plots the relationship between the average fluorescence at a pixel and the log p -value.

each pixel on a log scale versus the sample average fluorescence at the pixel. In general, evidence against the hypothesis increases as fluorescence decreases. Even though most low-fluorescence pixels do not show strong evidence against linear mixing, these results suggest caution when using linear unmixing methods for abundance estimation of low-fluorescence endmembers. For example, nearly all of the pixels of our replicate groundwater samples had fluorescence values less than 1 QSU, which is the range where approximately 40% of the violations of the linear mixing hypothesis are detected. We compared the results in Figure 4 that indicated significantly higher or lower fluorescence than expected under linear mixing with their corresponding EEMs (see Figure S2 in the Supporting Information). Significantly higher or lower fluorescence was found over a wide range of excitation (240-415 nm) but restricted to emission ≥ 500 nm for most mixtures. Two exceptions are noted, for m_2 and m_7 . In the case of m_2 , overestimation was found in the peak T region of protein-like fluorescence [Coble, 2007]. For m_7 , overestimation was found across a similar excitation range but at emission wavelengths ≥ 480 nm. However, examination of the EEMs in Figure S2 clearly show the majority of fluorescence occurs outside of the regions noted above where significantly higher or lower fluorescence was estimated. This indicates that despite being significant, these regions of over- or underestimation carry low information and do not contribute to the fluorescence signal used to identify sources in mixtures.

4.2 Experimental Variability of Abundance Estimates

The previous results indicated that there is not strong evidence against the linear mixing hypothesis for the vast majority of pixels of an EEM, especially pixels with high fluorescence intensities. However, estimation accuracy of endmember abundances relies not just on the linear mixing hypothesis, but also on the strength of the fluorescence signal relative to experimental noise. As our groundwater sample exhibits both a low signal-to-noise ratio, and has pixel intensities in the range where the linear mixing hypothesis is more suspect, we expect more difficulty in obtaining reliable abundance estimates for this low-fluorescence endmember.

Consider endmember abundance estimation for a mixed EEM y using noisy measured EEMs x^1, \dots, x^s , one from each of the endmembers of which y is assumed to be a mixture. Under the linear mixing hypothesis, the expectation of y is

$$E[y] = \Theta b = \theta^1 b_1 + \dots + \theta^s b_s$$

where b is the s -dimensional vector of abundances to be estimated and $\theta^1, \dots, \theta^s$ are hypothetical noiseless EEMs from each of the endmembers, so that $E[x^k] = \theta^k$ for $k = 1, \dots, s$. If Θ were known then a simple estimate of b would be the non-negative least squares estimate from the linear regression of y on Θ . As Θ is not observed, a simple alternative estimate \hat{b} of b is the non-negative least squares estimate of y on the matrix X having columns x^1, \dots, x^s .

The estimate \hat{b} of b will vary from experiment to experiment due to the variation of X around Θ and of y around Θb . In simple linear regression scenarios with independent, additive measurement noise with variance σ^2 , it is well-known that the variance of \hat{b} is given by $\text{Var}[\hat{b}] = (X^\top X)^{-1} \sigma^2$. Roughly speaking, the variance of \hat{b}_k , the k th element of \hat{b} , will be small if the magnitude of x^k , the k th column of X , is large relative to σ^2 , i.e. the signal to noise ratio is large. The situation for abundance estimation from fluorescence data is more complex, due to the multiple sources of multiplicative variation and the fact that x^1, \dots, x^s are themselves measured with noise. However, we still expect that the precision of abundance estimates will be positively related to the signal to noise ratio of the endmembers.

While we lack a simple formula for the variance of \hat{b} , it can still be assessed empirically if replicate EEMs are available, using the following resampling scheme which we illustrate in the context of the data from our study. For each of our $m = 7$ mixed samples, using non-negative least squares we regress one of the replicate mixed EEM vectors y on the matrix X consisting of one of the replicate groundwater EEMs, one of the replicate streamwater EEMs and one of the replicate wastewater EEMs. This generates a single estimate \hat{b} of b . We repeat this procedure for each of the $3 \times 3 \times 3 \times 3$ possible combinations of mixed and endmember EEMs, yielding 81 different estimates of b . The variation across these different estimates summarizes the effect of the experimental variability on the abundance parameter estimates.

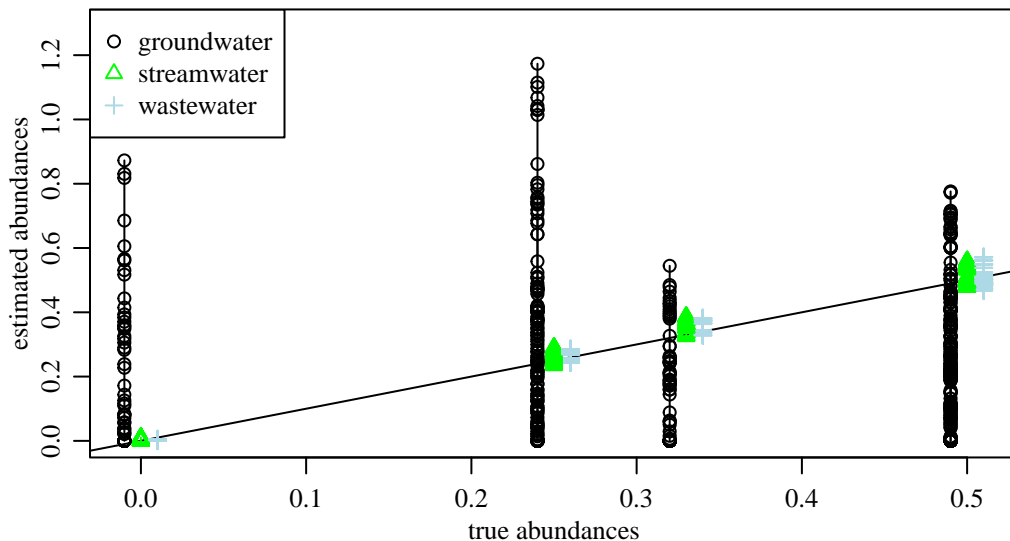


Figure 5: NNLS abundance estimates. Coefficients for stream, waste and groundwater given in green, blue and black respectively.

The results of this procedure are summarized graphically in Figure 5. Here, the parameter estimates for the abundances of the groundwater, streamwater and wastewater endmembers are given in black, green and blue respectively. The estimates for the stream and wastewater endmembers are very close to the true mixing proportions, and have a very narrow range across the combinations of replicate EEMs, indicating a high degree of accuracy in these estimates. In contrast, the groundwater abundance estimates have a very large range and thus low accuracy. The low signal to noise ratio of this endmember limits the precision to which its abundance in the mixture can be estimated.

These results are summarized further in Table 5. The columns give the true abundances b_1 , b_2 and b_3 for each mixture, as well as the sample mean and standard deviation of the 81 values for each of \hat{b}_1 , \hat{b}_2 and \hat{b}_3 . While the streamwater and wastewater estimates differ from the true mixing proportions slightly, they have low variance and are close enough for most applications. The groundwater estimates are not centered near the true mixing proportions, and the variance is high, indicating

	groundwater			streamwater			wastewater		
	b_1	mean(\hat{b}_1)	sd(\hat{b}_1)	b_2	mean(\hat{b}_2)	sd(\hat{b}_2)	b_3	mean(\hat{b}_3)	sd(\hat{b}_3)
m_1	0.00	0.153	0.228	0.50	0.496	0.009	0.50	0.491	0.014
m_2	0.50	0.386	0.197	0.50	0.517	0.022	0.00	0.003	0.001
m_3	0.50	0.169	0.224	0.00	0.004	0.004	0.50	0.537	0.028
m_4	0.25	0.337	0.370	0.25	0.250	0.007	0.50	0.497	0.017
m_5	0.25	0.227	0.193	0.50	0.531	0.027	0.25	0.268	0.013
m_6	0.50	0.198	0.162	0.25	0.272	0.014	0.25	0.268	0.014
m_7	0.33	0.158	0.166	0.33	0.358	0.020	0.33	0.361	0.019

Table 5: Mean and standard deviation of resampled NLS abundance estimates.

unreliability of abundance estimates for this endmember.

5 Discussion

A general class of EMMA methods for estimating endmember abundance assume some version of a linear mixing hypothesis – that is, the fluorescence properties of a mixed sample resemble the mixture of properties of its endmembers. Our study provides experimental credibility to these approaches, in that statistical tests failed to reject the linear mixing hypothesis for most pixels of several mixed EEMs, and in particular, pixels with high fluorescence levels. For DOM fluorescence, most unmixing methods have used derived parameters from fluorescence such as discrete “peak picking” [Coble, 2007, Goldman et al., 2012], the fluorescence index (FI; McKnight et al. [2001]), and/or the biological index (BIX) and humification index (HIX) [Huguet et al., 2009] to distinguish among samples, in addition to decomposition methods such as parallel factor analysis (PARAFAC) [Stedmon et al., 2003]. Employing DOM fluorescence in endmember mixing analysis has typically involved such peak-picking or PARAFAC decomposition [Larsen et al., 2015, Osburn et al., 2016], and often in combination [Lee et al., 2020]. As an alternative to using derived indices or PARAFAC components, Bryan et al. [2023] have shown how regressing the entire

vectorized EEM of a mixed sample on the EEMs of its endmembers can outperform other methods in terms of endmember abundance estimation. Our work provides support for the use of such direct linear estimation methods, as we were able to obtain highly accurate abundance estimates for high signal-to-noise endmembers using simple linear regression.

This work also demonstrates that replication is critically important for evaluating the validity and variability of an unmixing method’s estimated abundances. Variation in parameter estimates can arise due to a number of experimental factors. For example, a bandpass resolution setting on a fluorometer greater than the emission increment can make it difficult to resolve peak emission wavelength, leading to variation among replicates [Korak et al., 2014]. High scan rate settings on fluorometers often create noisy spectra, further introducing variation. Our fluorescence measurements were taken with 5 nm bandpass settings and 2 nm emission increments at a scan rate of 2400 nm/min. These parameters were optimized for measuring large numbers of samples – a consideration important to many studies using fluorescence – so it was encouraging that results showed linear mixing held in the regions of fluorescence containing the most signal, and therefore the most important information, despite this scan speed. It is possible that with lower scan speeds the variation in the groundwater endmember could be reduced.

In this work we have demonstrated how analysts can utilize replicates of discrete samples to measure experimental variation in their own laboratories. Such measures provide a means for statistical model evaluation (such as the linear mixing hypothesis) and assessments of estimation variability. In our study, we evaluated the linear mixing assumption over a range of fluorescence intensities commonly found in natural waters. We also showed that estimates of stream and wastewater abundances are highly accurate, whereas those for groundwater are highly variable across replications. Absent replication and the resulting quantification of experimental variation, this assessment would be unavailable - the differential accuracy of the abundance estimates across endmembers would be unknown.

References

- Yoav Benjamini and Yosef Hochberg. Controlling the false discovery rate: a practical and powerful approach to multiple testing. *J. Roy. Statist. Soc. Ser. B*, 57(1):289–300, 1995. ISSN 0035-9246.
- Ruchi Bhattacharya and Christopher L Osburn. Spatial patterns in dissolved organic matter composition controlled by watershed characteristics in a coastal river network: The Neuse River Basin, USA. *Water research*, 169:115248, 2020.
- Rasmus Bro. Parafac. tutorial and applications. *Chemometrics and intelligent laboratory systems*, 38(2):149–171, 1997.
- J.G. Bryan, P.D. Hoff, and C.L. Osburn. Routine estimation of dissolved organic matter sources using fluorescence data and linear least squares. *ACS ES&T Water*, 3(8):1972–2808, 2023. doi: 10.1021/acsestwater.2c00605. URL <https://doi.org/10.1021/acsestwater.2c00605>.
- J.G. Bryan, P.D. Hoff, and C.L. Osburn. Linear source apportionment using generalized least squares. *Technometrics*, to appear, 2024.
- Paula G Coble. Marine optical biogeochemistry: the chemistry of ocean color. *Chemical reviews*, 107(2):402–418, 2007.
- Morgane Derrien, Min-Seob Kim, Giyoung Ock, Seongjin Hong, Jinwoo Cho, Kyung-Hoon Shin, and Jin Hur. Estimation of different source contributions to sediment organic matter in an agricultural-forested watershed using end member mixing analyses based on stable isotope ratios and fluorescence spectroscopy. *Science of the Total Environment*, 618:569–578, 2018.
- Jason B Fellman, Eran Hood, and Robert GM Spencer. Fluorescence spectroscopy opens new windows into dissolved organic matter dynamics in freshwater ecosystems: A review. *Limnology and oceanography*, 55(6):2452–2462, 2010.

- John R Gilchrist and Darren M Reynolds. Optical spectroscopy instrumentation design, quality assurance, and control: Bench-top fluorimetry. *Aquatic Organic Matter Fluorescence*, page 147, 2014.
- Jami H Goldman, Stewart A Rounds, and Joseph A Needoba. Applications of fluorescence spectroscopy for predicting percent wastewater in an urban stream. *Environmental Science & Technology*, 46(8):4374–4381, 2012.
- Arnaud Huguet, Lilian Vacher, Stéphane Relexans, Sylvain Saubusse, Jean-Marie Froidefond, and Edith Parlanti. Properties of fluorescent dissolved organic matter in the gironde estuary. *Organic Geochemistry*, 40(6):706–719, 2009.
- Shreeram Inamdar. The use of geochemical mixing models to derive runoff sources and hydrologic flow paths. In *Forest hydrology and biogeochemistry: synthesis of past research and future directions*, pages 163–183. Springer, 2011.
- Julie A Korak, Aaron D Dotson, R Scott Summers, and Fernando L Rosario-Ortiz. Critical analysis of commonly used fluorescence metrics to characterize dissolved organic matter. *Water research*, 49:327–338, 2014.
- Dolly N Kothawala, Kathleen R Murphy, Colin A Stedmon, Gesa A Weyhenmeyer, and Lars J Tranvik. Inner filter correction of dissolved organic matter fluorescence. *Limnology and Oceanography: Methods*, 11(12):616–630, 2013.
- Laurel Larsen, Jud Harvey, Katherine Skalak, and Marissa Goodman. Fluorescence-based source tracking of organic sediment in restored and unrestored urban streams. *Limnology and Oceanography*, 60(4):1439–1461, 2015.
- Mi-Hee Lee, Christopher L Osburn, Kyung-Hoon Shin, and Jin Hur. New insight into the applicability of spectroscopic indices for dissolved organic matter (DOM) source discrimination in aquatic systems affected by biogeochemical processes. *Water Research*, 147:164–176, 2018.
- Mi-Hee Lee, Seung Yoon Lee, Ha-Young Yoo, Kyung-Hoon Shin, and Jin Hur. Comparing optical versus chromatographic descriptors of dissolved organic matter

- (DOM) for tracking the non-point sources in rural watersheds. *Ecological Indicators*, 117:106682, 2020.
- Philippe Massicotte, Eero Asmala, Colin Stedmon, and Stiig Markager. Global distribution of dissolved organic matter along the aquatic continuum: Across rivers, lakes and oceans. *Science of the Total Environment*, 609:180–191, 2017.
- Diane M McKnight, Elizabeth W Boyer, Paul K Westerhoff, Peter T Doran, Thomas Kulbe, and Dale T Andersen. Spectrofluorometric characterization of dissolved organic matter for indication of precursor organic material and aromaticity. *Limnology and Oceanography*, 46(1):38–48, 2001.
- Kathleen R Murphy, Kenna D Butler, Robert GM Spencer, Colin A Stedmon, Jennifer R Boehme, and George R Aiken. Measurement of dissolved organic matter fluorescence in aquatic environments: an interlaboratory comparison. *Environmental science & technology*, 44(24):9405–9412, 2010.
- Christopher L Osburn, Lauren T Handsel, Benjamin L Peierls, and Hans W Paerl. Predicting sources of dissolved organic nitrogen to an estuary from an agro-urban coastal watershed. *Environmental science & technology*, 50(16):8473–8484, 2016.
- R Core Team. *R: A Language and Environment for Statistical Computing*. R Foundation for Statistical Computing, Vienna, Austria, 2024. URL <https://www.R-project.org/>.
- Colin A Stedmon and Norman B Nelson. The optical properties of DOM in the ocean. In *Biogeochemistry of marine dissolved organic matter*, pages 481–508. Elsevier, 2015.
- Colin A Stedmon, Stiig Markager, and Rasmus Bro. Tracing dissolved organic matter in aquatic environments using a new approach to fluorescence spectroscopy. *Marine chemistry*, 82(3-4):239–254, 2003.

Henry F Wilson and Marguerite A Xenopoulos. Effects of agricultural land use on the composition of fluvial dissolved organic matter. *Nature Geoscience*, 2(1):37–41, 2009.

Supporting Information

S.1 Absorbance and fluorescence parameters

		$a_{254} (m^{-1})$			$a_{350} (m^{-1})$			$a_{440} (m^{-1})$			$S_{300-650} (\mu m^{-1})$		
Sample	n	mean	std	sem	mean	std	sem	mean	std	sem	mean	std	sem
s_1	3	1.400	0.590	0.340	0.73	0.44	0.25	0.37	0.19	0.11	16.80	7.16	4.13
s_2	3	28.980	0.530	0.310	7.92	0.41	0.24	1.88	0.13	0.08	15.58	0.20	0.12
s_3	3	56.570	0.100	0.060	8.10	0.12	0.07	3.19	0.07	0.04	15.35	0.39	0.23
m_1	3	43.510	1.800	1.040	8.19	0.96	0.55	2.72	0.30	0.17	15.03	0.47	0.27
m_2	3	15.450	0.620	0.360	4.13	0.78	0.45	1.22	0.11	0.07	15.35	0.36	0.21
m_3	3	29.560	0.590	0.340	5.04	0.45	0.26	1.87	0.12	0.07	14.52	0.32	0.19
m_4	3	36.050	0.290	0.170	6.66	0.10	0.06	2.24	0.13	0.08	14.97	0.40	0.23
m_5	3	29.030	0.810	0.460	6.24	0.43	0.25	1.94	0.19	0.11	15.19	0.40	0.23
m_6	3	21.970	1.180	0.680	4.46	0.77	0.44	1.48	0.10	0.06	14.92	0.10	0.06
m_7	3	29.790	1.150	0.660	5.75	0.71	0.41	1.87	0.16	0.09	15.14	0.26	0.15
		S_R			Fl			BIX			HIX		
Sample	n	mean	std	sem	mean	std	sem	mean	std	sem	mean	std	sem
s_1	3	0.813	0.926	0.535	1.38	0.74	0.42	1.77	0.80	0.46	3.88	3.56	2.06
s_2	3	0.803	0.001	0.001	1.35	0.03	0.02	0.75	0.02	0.01	5.18	0.12	0.07
s_3	3	2.979	0.074	0.043	1.70	0.04	0.02	0.84	0.05	0.03	0.46	0.01	0.01
m_1	3	1.947	0.028	0.016	1.56	0.08	0.04	0.79	0.00	0.00	1.01	0.00	0.00
m_2	3	0.859	0.048	0.028	1.34	0.04	0.02	0.74	0.03	0.01	5.11	0.05	0.03
m_3	3	2.841	0.158	0.091	1.74	0.30	0.18	0.89	0.04	0.02	0.46	0.01	0.01
m_4	3	2.257	0.060	0.035	1.58	0.16	0.09	0.83	0.05	0.03	0.76	0.03	0.02
m_5	3	1.559	0.074	0.042	1.50	0.13	0.07	0.83	0.05	0.03	1.44	0.02	0.01
m_6	3	1.872	0.004	0.002	1.48	0.20	0.12	0.83	0.01	0.01	1.03	0.00	0.00
m_7	3	1.896	0.088	0.051	1.52	0.10	0.06	0.79	0.03	0.02	1.02	0.02	0.01

Table S1: Absorbance and fluorescence parameters for the samples used in this study.

S.2 Example EEMs

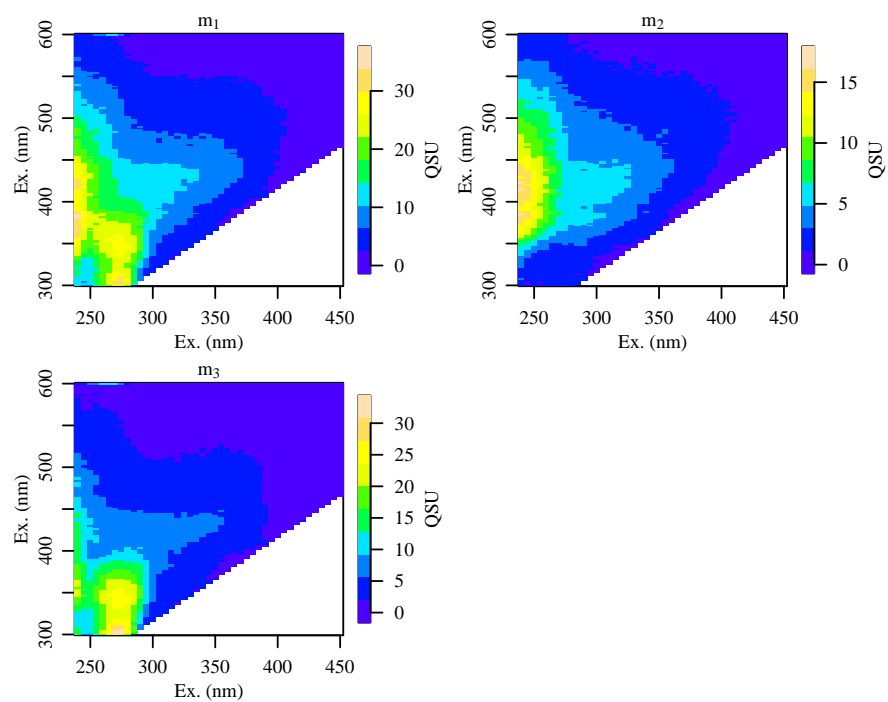


Figure S1: One replicate EEM from each of the endmember water samples s_1 , s_2 , s_3 .

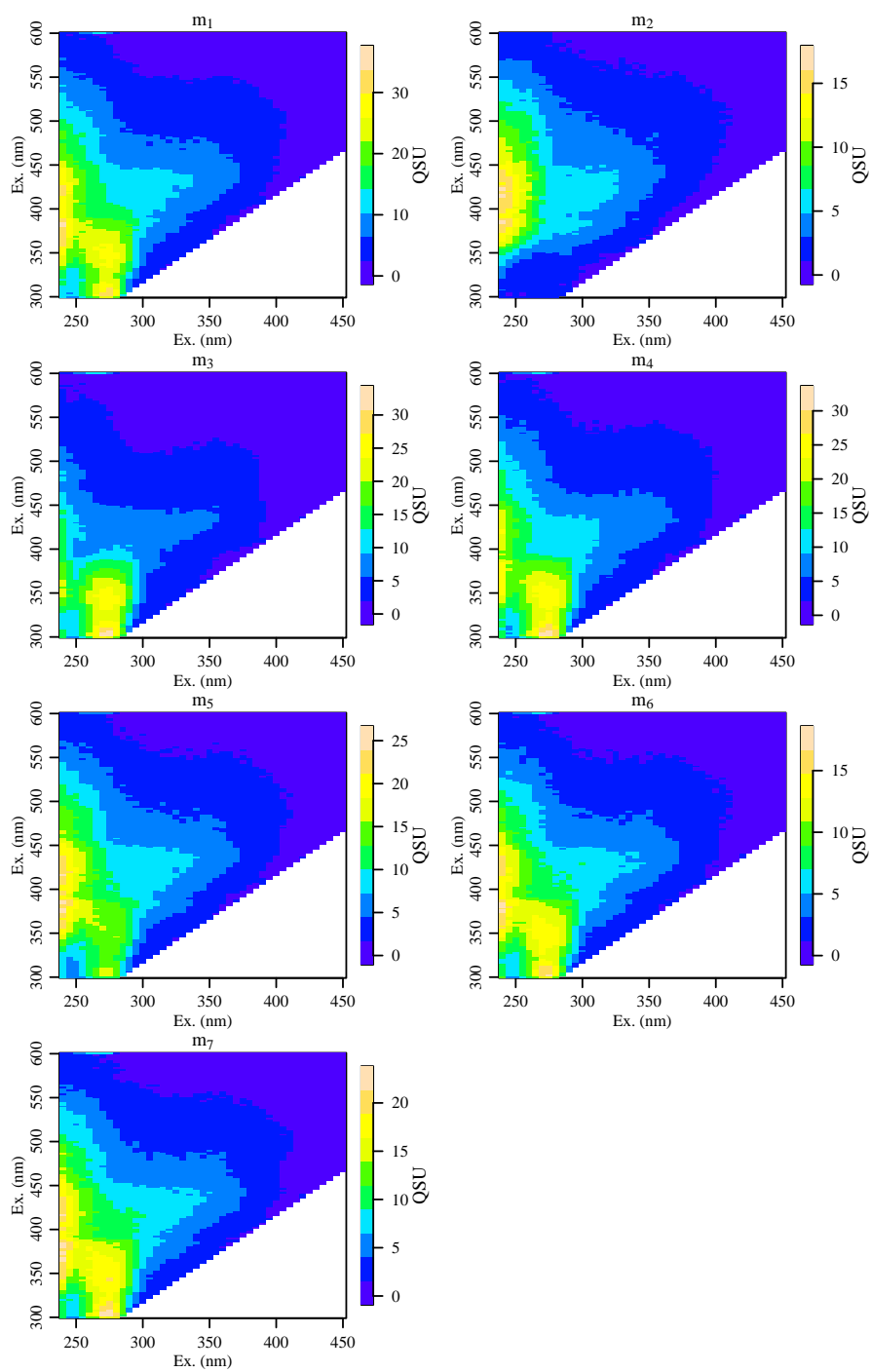


Figure S2: One replicate EEM from each of the mixed water samples m_1, \dots, m_7 .

S.3 Derivation of the linear mixing test statistic

We evaluate the hypothesis $H_j : \mu_j = \theta_j \cdot b$ with the test statistic $z_j = (\hat{\mu}_j - \hat{\theta}_j \cdot b) / \hat{\sigma}_j$, where

- $\hat{\mu}_j = \bar{y}_j = \sum_{i=1}^n y_{i,j} / n$, the across-replicate average fluorescence at pixel j ;
- $\hat{\theta}_j = (\bar{x}_j^1, \dots, \bar{x}_j^s)$, where $\bar{x}_j^k = \sum_{i=1}^n x_{i,j}^k / n$, the across-replicate average fluorescence at pixel j for endmember k , $k = 1, \dots, s$.
- $\hat{\sigma}_j$ is an estimate of the standard deviation of $\hat{\mu}_j - \hat{\theta}_j \cdot b$.

To compute $\hat{\sigma}_j$, we first find the variance σ_j^2 of $\hat{\mu}_j - \hat{\theta}_j \cdot b$. Using standard formulas for variances of sums, we have

$$\begin{aligned} \sigma_j^2 &= \text{Var}[\hat{\mu}_j - \hat{\theta}_j \cdot b] = \text{Var}[\bar{y}_j - \bar{x}_j \cdot b] \\ &= \text{Var}[\bar{y}_j] + \sum_{k=1}^s b_k^2 \text{Var}[\bar{x}_j^k]. \end{aligned} \quad (3)$$

Under the multiplicative model the variance of \bar{y}_j for a sample size of n can be computed from Equation 2 as follows:

$$\text{Var}[\bar{y}_j] = \text{Var}[y_{i,j}] / n = \mu_j^2 ((\sigma_a^2 + 1)(\sigma_e^2 + 1) - 1) / n. \quad (4)$$

Similarly,

$$\text{Var}[\bar{x}_j^k] = \text{Var}[x_{i,j}^k] / n = (\theta_j^k)^2 ((\sigma_a^2 + 1)(\sigma_e^k)^2 + 1) - 1) / n. \quad (5)$$

where here $\sigma_e^1, \dots, \sigma_e^s$ refer to the endmember-specific measurement standard deviations described in Section 3.2. An estimate $\hat{\sigma}_j^2$ of σ_j^2 is then obtained by first replacing in Equations 4 and 5 the unknown values of μ_j , $\theta_j^1, \dots, \theta_j^s$, σ_a^2 and the σ_e^2 's with the estimates described in Section 3. The results are then plugged into the formula in Equation 3 to obtain the estimate $\hat{\sigma}_j^2$ of σ_j^2 . The denominator $\hat{\sigma}_j$ of the statistic z_j is the square-root of $\hat{\sigma}_j^2$. Numerical examples of this calculation can be found in the replication material for this article.